J Appl Electrochem (2007) 37:971–982
DOI 10.1007/s10800-007-9337-x

ORIGINAL PAPER

A thin-film/agglomerate model of a proton-exchange-membrane fuel cell cathode catalyst layer with consideration of solid-polymer-electrolyte distribution

Ken-Ming Yin

Received: 17 June 2006 / Revised: 13 April 2007 / Accepted: 30 April 2007 / Published online: 26 May 2007

Abstract A thin-film/agglomerate model for the cathode part of a proton-exchange-membrane fuel cell is developed. Parameter estimation is employed to determine the exchange current density in the catalyst layer, proton conductivity of the recast ionomer, and oxygen diffusivity in the solid polymer electrolyte. The effects of catalyst and polymer electrolyte loadings in the catalyst layer on the cell performance are demonstrated using this model. The influence of polymer electrolyte distribution in the catalyst layer is correlated with the oxygen diffusion and proton migration rates within the electrolyte. It is found that proton migration in the polymer electrolyte is the dominant factor for cell current density under normal operating conditions. A better cell performance is achieved by a concentrated polymer electrolyte near the catalyst layer/membrane interface.

Keywords Cathode catalyst layer · Mathematical model · Proton-exchange-membrane fuel cell · Solid polymer electrolyte · Thin-film/agglomerate model

List of Symbols

a_e	gas/electrolyte interfacial area per unit volume in the catalyst layer, cm^{-1}
a_s	catalytic area per platinum mass, $cm^2\ g^{-1}$
a_v	active area per unit volume of Pt/C/electrolyte mixture region, cm^{-1}
C_A	dissolved oxygen concentration in the solid polymer electrolyte, mol cm^{-3}
C_{Ag}	oxygen gas concentration, mol cm^{-3}
$C_{Ag,bulk}$	bulk O_2 concentration in the cathode channel, mol cm^{-3}
$C_{A,ref}$	reference dissolved oxygen concentration (= $P_{A,ref}/(K_A RT)$), mol cm^{-3}
C_{A0}	dissolved oxygen concentration at gas/electrolyte interface, mol cm^{-3}
$C_{A\delta}$	oxygen concentration at $y = \delta$ in Fig. 1, mol cm^{-3}
$C_{H+,ref}$	reference proton concentration in the electrolyte, mol dm^{-3}
D	diffusivity of oxygen in the electrolyte, $cm^2\ s^{-1}$
D^{eff}	effective diffusivity of oxygen in ionomer phase of the catalyst layer, $cm^2\ s^{-1}$
D_g	diffusivity of oxygen gas, $cm^2\ s^{-1}$
D_g^{eff}	effective diffusivity of oxygen gas in the catalyst layer, $cm^2\ s^{-1}$
D_{ga}^{eff}	gas phase effective diffusivity in an agglomerate ($\delta_n < y < \delta$ in Case II, shown in Fig. 1c), $cm^2\ s^{-1}$
D_{gd}^{eff}	effective O_2 diffusivity in the gas diffuser, $cm^2\ s^{-1}$
D_{H+}	proton diffusivity in the ionomer phase, $cm^2\ s^{-1}$
E	local potential (= $V - \Phi$), V
E_c	electrode potential (= $V - \Phi_{RE}$), V
F	Faraday constant, 96,500 C mol^{-1}
i	local ionic current density in the catalyst layer, A cm^{-2}
I	cell current density, A cm^{-2}
I_{lim}	limiting current density, A cm^{-2}
$I_{c,lim}$	current density defined in Eq. B8, A cm^{-2}
$I_{d,lim}$	current density defined in Eq. B9, A cm^{-2}
$j_{o,ref}$	exchange current density of oxygen reduction at the reference concentration, A cm^{-2}
k	rate constant of oxygen reduction defined in Eq. 22, cm s^{-1}

K.-M. Yin (✉)
Department of Chemical Engineering and Materials Science, Yuan-Ze University, Chung-Li, Taoyuan 32003, Taiwan, ROC
e-mail: cekenyin@saturn.yzu.edu.tw

K_A oxygen solubility in the polymer electrolyte, cm^3 mol^{-1}
L_c thickness of the catalytic layer, cm
L_d thickness of the gas diffuser, cm
L_m thickness of Nafion® membrane, cm
m parameter defined in Eq. B4, cm^{-1}
m_n solid polymer electrolyte loading, g cm^{-2}
m_{Pt} Pt loading, g cm^{-2}
M_A molecular weight of gas component A, g mol^{-1}
M_B molecular weight of gas component B, g mol^{-1}
n number of electron transferred in reaction 1 (= 4)
n_s number of slabs per cross sectional area in the catalyst layer defined in Eq. A1, cm^{-1}
N_{Ax} oxygen gas molar flux in the axial direction, mol cm^{-2} s^{-1}
N_{Ay} dissolved oxygen molar flux perpendicular to the slab surface, mol cm^{-2} s^{-1}
$P_{A,ref}$ reference oxygen partial pressure, atm
P_{CA} critical pressure of gas component A, atm
P_{CB} critical pressure of gas component B, atm
P_t total gas pressure, atm
R universal gas constant, 8.314 J $mol^{-1}K^{-1}$ in Eqs. 22, 24, and 25; 82.06atm cm^3 $mol^{-1}K^{-1}$ in Eq. 14.
T cell temperature, K
T_{CA} critical temperature of gas component A, K
T_{CB} critical temperature of gas component B, K
U_o standard open circuit potential of oxygen reduction, V
U_{ref} open circuit potential of oxygen reduction at the reference concentration, V
V potential of solid carbon matrix phase, V
w weight percentage of Pt in the carbon supported Pt/C catalyst

Greek letters

α transfer coefficient of oxygen reduction
δ dimension of the agglomerate slab, cm
δ_f polymer electrolyte film thickness that covers the agglomerate(δ_n–δ), depicted in Fig. 1b, cm
δ_n polymer electrolyte occupied thickness in the agglomerate slab, shown in Fig. 1b, c, cm
δ_t one-half distance between center lines of two agglomerate slabs, shown in Fig. 1, cm
ε_a void fraction of the electrolyte phase within an agglomerate
ε_d gas fraction in the gas diffuser
Φ potential in the polymer electrolyte, V
Φ_{RE} electrolyte potential at the reference position $x = L_c + L_m$, V
η electrode over-potential, V
κ_m conductivity in the electrolyte phase, S cm^{-1}
κ_m^{eff} effective ionic conductivity in the catalyst layer, S cm^{-1}
ρ_c carbon density, g cm^{-3}
ρ_n electrolyte density, g cm^{-3}
ρ_{pt} platinum density, g cm^{-3}

1 Introduction

Experimental work on the proton-exchange-membrane fuel cell (PEMFC) has revealed that a better utilization of carbon supported platinum catalyst (Pt/C) hinges on an appropriate composition of the solid polymer electrolyte (SPE) and the preparation procedure of the gas diffusion electrode (GDE) [1–12]. GDE is prepared by a porous carbon fiber matrix named gas diffusion layer (GDL), on which a thin catalyst layer (CL) of Pt/C aggregates impregnated with the recast Nafion® electrolyte is covered. Occasionally, a micro-layer of hydrophobic treated carbon paste is added between the catalyst layer and the gas diffusion layer to assist the repulsion of water that generated on the cathode electrode [13, 14]. Two common procedures are adopted to incorporate Nafion electrolyte in the catalyst layer: (i) Pt/C is pre-mixed with dilute Nafion solution as a catalyst slurry, which is to be brushed or spread onto the GDL to form a complete GDE [2, 4, 6]; (ii) GDL is pre-coated with a catalyst layer of Pt/C or hydrophobic-treated Pt/C/PTFE, followed by the heat treatment. Nafion® electrolyte is then brushed or sprayed onto the GDL surface [1, 2, 7]. Apparently, the second approach induces a concentrated solid polymer electrolyte near one side of the CL surface, and the resultant composition variation across the CL may have certain effect on the cell I–V behavior [2, 7]. The prepared anode and cathode GDEs by either method are to be hot-pressed with a Nafion® membrane (M) in between to complete the sandwiched membrane-electrode-assembly (MEA).

In parallel with the experimental studies on GDE fabrication, theoretical models were developed to explore the cell performance with regard to the electrode morphology and chemical composition in the GDE, as reviewed by Cheddie and Munroe [15]. Much research has focused on the cathode GDE due to the larger activation resistance of oxygen reduction as compared to the anode hydrogen oxidation [16]. Bernardi and Verbrugge [17, 18] proposed a cathode GDE model where a uniform Pt/C/SPE composite structure is treated as a pseudo-homogeneous mixture in the catalyst layer. Dissolved oxygen in the SPE is diffused and reduced through the CL at the presence of proton. Since no gas void is considered in their study,

electrochemical reaction is compelled to the interface of GDL/CL due to the low solubility and slow diffusion of oxygen in the electrolyte. A modified homogeneous model was given by Springer et al.[19], where oxygen permeability was much raised to conform to the experimentally observed polarization curve. The increase in permeability was explained by ''the possibility of significant oxygen diffusion along the grain boundaries of carbon/electrolyte composite in the catalyst layer.'' The predicted reaction rate by Springer et al. is higher near the catalyst layer/membrane (CL/M) interface instead. It is likely the gaseous oxygen mass transport do occur within the cathode CL. The exceedingly high gas diffusion from GDL/CL over the proton migration from CL/M compels oxygen reduction near the CL/M interface. Other homogeneous model was given by Wang et al. [20] and Hsuen [21], in which the CL comprises a Pt/C/SPE/gas homogeneous mixture; the oxygen solubility equilibrium preserves between the gas and electrolyte phases within the CL. In the work of Wang et al. [20], the percolation theory was incorporated to account for the random nature of the catalyst layer. Their results revealed that for a three sub-layered structure with higher Nafion content on the membrane side exhibits enhanced cell performance.

The mass transport of both gaseous and dissolved oxygen, proton migration, and the associated electrochemical reaction within the CL are better described by the heterogeneous model in view of the actual morphological observations [22, 23]. That is, nano-sized platinum particles (2–3 nm) covered carbon powders (~30 nm) are normally aggregated to form larger secondary clusters (~100 nm) impregnated with Nafion polymer electrolyte [24]. The aspect ratio of Pt/C geometric dimensions and the associated ionomer distribution have impacts on the oxygen diffusion within the electrolyte and alter the reaction distribution within the agglomerates. The thin-film/agglomerate model proposed by Springer and Raistrick [25, 26] grasps the important finite dimension features, which is easier to be implemented as compared to other more complicated spherical [22, 23, 27–31] and cylindrical agglomerate models [32–34].

The present work is focused on the influence of Pt loading and SPE distribution on the performance of a PEMFC using a simple thin-film agglomerate model. The catalyst layer is considered to be composed of many parallel slabs that contain numerous carbon supported platinum catalysts immersed within the SPE as shown in Fig. 1. Two situations need to be considered with regard to the SPE loading: (i) The existence of external oxygen diffusion barrier within the electrolyte film caused by the flooded SPE (Fig. 1b). (ii) The less than fully utilized Pt/C catalytic surface area due to the insufficient impregnation of SPE (Fig. 1c). In addition, the consequence of non-uniformly distributed Nafion electrolyte within the CL caused by the different GDE fabrication procedures is elucidated.

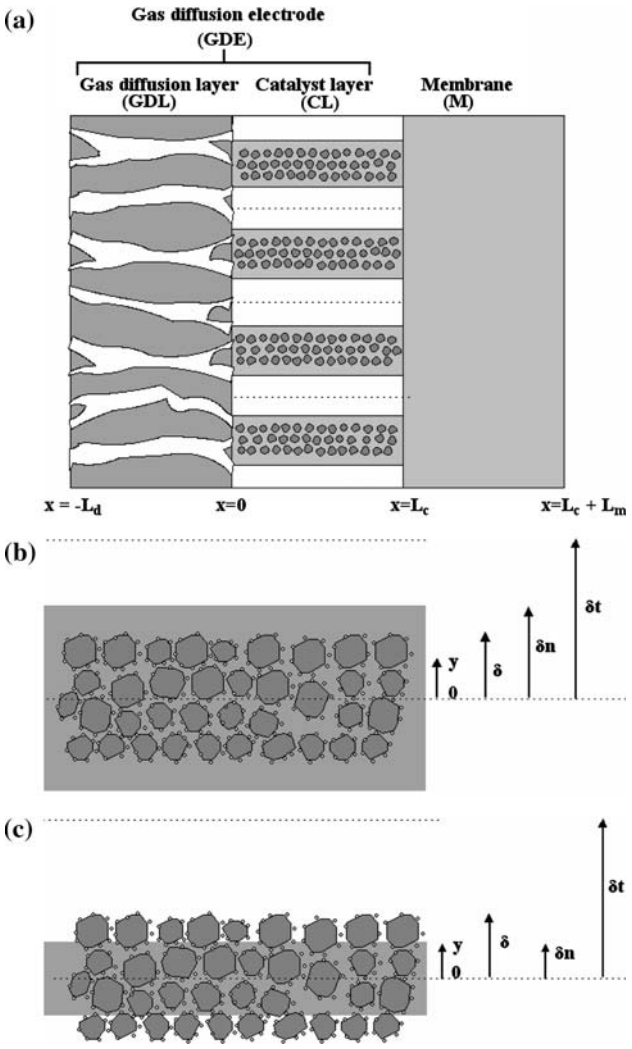

Fig. 1 (**a**) Schematic of the cathode part of MEA (not to scale); (**b**) Details of the SPE impregnated Pt/C clusters when Nafion is flooded over the agglomerate slabs (Case I); (**c**) Details of the SPE impregnated Pt/C clusters that is less than fully filled electrolyte in the voids so that not all the catalytic platinum surface is utilized (Case II)

2 Mathematical model

2.1 Modeling domain and assumptions

Depicted in Fig. 1a, the hydrated polymer membrane (M) serves as the separator, across which proton migrates from the anode CL into the cathode CL. Protons are migrate and react with the dissolved oxygen on the surface of Pt/C clusters within the catalyst layer, according to the reaction:

$$4H^+ + O_2 + 4e^- \rightarrow 2H_2O \quad (1)$$

Recast Nafion electrolyte serves as the proton conveyor, binds Pt/C particles firmly within the catalyst layer, and adheres with the adjacent layers of polymer membrane (M) and the gas diffusion layer (GDL).

Gas phase oxygen assumes to be transported only in the axial direction, while the dissolved oxygen is diffused perpendicular to the catalyst slabs. The system is assumed to be isothermal with the following assumptions: (i) Water vapor and possible water liquid phase are not considered in the catalyst layer or gas diffuser. That is, only oxygen and nitrogen are included in the model. (ii) Recast polymer electrolyte phase is fully hydrated with constant proton conductivity. Possible dry effect is not included either.

2.2 Case I: sufficient polymer electrolyte forming an external thin film on the surface of the slab

2.2.1 *Mass conservation of oxygen*

For the model region shown in Fig. 1b, the mass conservation of dissolved oxygen in the region of Pt/C/SPE mixture ($0 \leq y \leq \delta$) is expressed as:

$$\frac{dN_{Ay}}{dy} + kC_A = 0 \quad (2)$$

where N_{Ay} is the dissolved oxygen molar flux perpendicular to the slab surface, k the potential dependent rate constant. N_{Ay} is expressed according to Fick's law:

$$N_{Ay} = -D^{eff}\frac{dC_A}{dy}. \quad (3)$$

The effective diffusivity of oxygen within the agglomerate, D^{eff}, is the bulk diffusivity D corrected by the void fraction ε_a using the Bruggeman relation [16]

$$D^{eff} = D\varepsilon_a^{1.5} \quad (4)$$

Eq. 2 can be solved with the boundary conditions: $\frac{dC_A}{dy} = 0$ at $y = 0$, and $C_A = C_{A\delta}$ at $y = \delta$ according to Fig. 1b.

$$\frac{C_A}{C_{A\delta}} = \frac{\cosh\left(\sqrt{\frac{k}{D^{eff}}}\,y\right)}{\cosh\left(\sqrt{\frac{k}{D^{eff}}}\,\delta\right)} \quad (5)$$

The oxygen concentration and flux within the external SPE thin-film ($\delta < y < \delta_n$) of an agglomerate slab are expressed in Eqs. 6 and 7, respectively

$$C_A = C_{A\delta} + \frac{C_{A0} - C_{A\delta}}{\delta_n - \delta}(y - \delta) \quad (6)$$

$$N_{Ay} = -D\frac{C_{A0} - C_{A\delta}}{\delta_n - \delta} \quad (7)$$

In which C_{A0} is the dissolved oxygen concentration at gas/electrolyte interface ($y = \delta_n$). $C_{A\delta}$ is determined by the constraint of flux continuity at $y = \delta$. That is, oxygen flux calculated from Eq. 3 should be equal to that in Eq. 7. Once $C_{A\delta}$ determined, the oxygen flux at gas/electrolyte interface ($y = \delta_n$) can be expressed:

$$N_{Ay}\big|_{y=\delta_n} = \frac{-C_{A0}\sqrt{kD^{eff}}\tanh\left(\sqrt{\frac{k}{D^{eff}}}\delta\right)}{1 + \frac{\delta_n - \delta}{D}\sqrt{kD^{eff}}\tanh\left(\sqrt{\frac{k}{D^{eff}}}\delta\right)} \quad (8)$$

Mass conservation of oxygen gas in the axial direction gives:

$$\frac{dN_{Ax}}{dx} - N_{Ay}\big|_{y=\delta_n} n_s = 0 \quad (9)$$

where n_s is the number of slabs per unit cross sectional area.$N_{Ax}$is driven by the diffusion mass transfer:

$$N_{Ax} = -D_g^{eff}\frac{dC_{Ag}}{dx} \quad (10)$$

D_g^{eff} is the effective gaseous oxygen diffusivity modified with gas void fraction using the Bruggeman relation:

$$D_g^{eff} = D_g\left(\frac{\delta_t - \delta_n}{\delta_t}\right)^{1.5} \quad (11)$$

For a binary gas mixture, diffusivity D_g can be calculated using the Slattery and Bird formula [35]:

$$P_t D_g = 0.0002745\left(\frac{T}{\sqrt{T_{CA}T_{CB}}}\right)^{1.823}(P_{CA}P_{CB})^{1/3}(T_{CA}T_{CB})^{5/12}\left(\frac{1}{M_A} + \frac{1}{M_B}\right)^{1/2} \quad (12)$$

In combination of Eqs. 8–10, Eq. 13 can be derived to determine the gaseous oxygen concentration C_{Ag} across the CL.

$$D_g^{eff}\frac{d^2C_{Ag}}{dx^2} - \frac{\frac{C_{Ag}}{K_A}n_s\sqrt{kD^{eff}}\tanh\left(\sqrt{\frac{k}{D^{eff}}}\delta\right)}{1 + \frac{\delta_n - \delta}{D}\sqrt{kD^{eff}}\tanh\left(\sqrt{\frac{k}{D^{eff}}}\delta\right)} = 0 \quad (13)$$

K_A is the solubility of oxygen in the SPE [16]

$$K_A = \frac{1}{RT}\exp\left(-\frac{666}{T} + 14.1\right) \tag{14}$$

2.2.2 Current conservation

Ionic current density is expressed as

$$i = \kappa_m^{eff}\frac{dE}{dx} \tag{15}$$

where $E = V$–Φ. Note κ_m^{eff} is the effective ionomer conductivity:

$$\kappa_m^{eff} = \kappa_m\left(\frac{\delta_n - \delta(1-\varepsilon_a)}{\delta_t}\right)^{1.5} \tag{16}$$

The local transfer current density, di/dx, is related to the variation in O_2 gas flux within the catalyst layer.

$$\frac{di}{dx} = -nFD_g^{eff}\frac{d^2C_{Ag}}{dx^2} \tag{17}$$

n is the number of electrons transferred in oxygen reduction. In combination of Eqs. 15 and 17, one has

$$\frac{\kappa_m^{eff}}{nF}\frac{d^2E}{dx^2} + D_g^{eff}\frac{d^2C_{Ag}}{dx^2} = 0 \tag{18}$$

2.3 Case II: Less than fully utilized Pt/C surface area due to insufficient SPE

2.3.1 Mass conservation of oxygen

A similar procedure regarding oxygen mass conservation is applied to Case II as shown in Fig. 1c:

$$D_g^{eff}\frac{d^2C_{Ag}}{dx^2} - \frac{\frac{C_{Ag}}{K_A}n_s\sqrt{kD^{eff}}\tanh\left(\sqrt{\frac{k}{D^{eff}}}\delta_n\right)}{1 + \frac{\delta-\delta_n}{D_{ga}^{eff}K_A}\sqrt{kD^{eff}}\tanh\left(\sqrt{\frac{k}{D^{eff}}}\delta_n\right)} = 0 \tag{19}$$

D_{ga}^{eff} is the gas phase effective diffusivity within the SPE un-filled space of the catalyst slab ($\delta_n < y < \delta$): $D_{ga}^{eff} = D_g\varepsilon_a^{1.5}$, and

$$D_g^{eff} = D_g\left(\frac{\delta_t - \delta}{\delta_t}\right)^{1.5} \tag{20}$$

2.3.2 Current conservation

Equation 18 is adopted for the current conservation equation for the Case II, while the effective conductivity is modified by

$$\kappa_m^{eff} = \kappa_m\left(\frac{\delta_n\varepsilon_a}{\delta_t}\right)^{1.5} \tag{21}$$

2.4 Kinetic expression

The rate constant k shown in Eq. 2 is electrode over-potential dependent with the Tafel expression [36]:

$$k = \frac{a_v j_{o,ref}}{n\,FC_{A,ref}}\exp\left(\frac{-\alpha F\eta}{RT}\right) \tag{22}$$

a_v is the active surface area per unit volume in the Pt/C/electrolyte mixed region, $j_{o,ref}$ the reference exchange current density corresponding to the reference concentration $C_{A,ref}$, α the cathodic transfer coefficient, R the universal gas constant, F the Faraday constant, and T the absolute temperature. The electrode over potential η is correlated with the electrode potential V, the SPE potential Φ, and the reference open circuit voltage of oxygen reaction U_{ref}:

$$\eta = V - \Phi - U_{ref} \tag{23}$$

U_{ref} corresponds to the reference O_2 pressure $P_{A,ref}$ (=1 atm) and reference H^+ concentration $C_{H+,ref}$:

$$U_{ref} = U_o + \frac{RT}{F}\ln\left(P_{A,ref}^{1/4}C_{H^+,ref}\right) \tag{24}$$

U_o is the standard open circuit voltage of oxygen reaction. $C_{H+,ref}$ can be determined once the ionomer conductivity κ_m and the proton diffusivity D_{H+} are available [17]:

$$\kappa_m = \frac{F^2}{RT}D_{H^+}\frac{C_{H^+,ref}}{1,000} \tag{25}$$

A factor of 1,000 is needed to convert the units of $C_{H+,ref}$ from mol dm^{-3} to mol cm^{-3}.

2.5 Numerical methods

The governing equations and associated boundary conditions to be solved are summarized in Table 1. The solution scheme is developed for a potentiostatic mode for a given potential E_c(=V–Φ_{RE}), where Φ_{RE} is the electrolyte potential at $x = L_c + L_m$, set arbitrarily to zero as reference. The set of equations is solved using subroutine BAND [37]. Kinetic parameters: ionomer conductivity κ_m, oxygen diffusivity in the polymer phase D, and the exchange current density $j_{o,ref}$, were estimated by fitting to the experimental data using subprogram DLSARG based on the Levenberg-Marquardt optimization algorithm [38]. The minimization function is defined as

Table 1 Summary of equations solved using BAND [37]

Dependent variables	Governing equations	Boundary conditions ($x = 0$)	Boundary conditions ($x = L_c$)
C_{Ag}	Eq. 13 or 19	$C_{Ag} = C_{Ag,bulk} + \frac{IL_d}{nFD_{gd}^{eff}}$ [a]	$dC_{Ag}/dx = 0$
E	Eq. 18	$dE/dx = 0$	$E = E_c - \frac{IL_m}{\kappa_m}$ [b]
I	$dI/dx = 0$	$dI/dx = 0$	$i–I = 0$
i	Eq. 15	$i = 0$	Eq. 15

[a] L_d is the gas diffuser thickness, and D_{gd}^{eff} the effective O_2 diffusivity in the diffuser corrected for the gas void fraction ε_d using Bruggeman relation [16]

[b] $E_c = V - \Phi_{RE}$. Φ_{RE} is electrolyte potential at $x = L_m + L_c$, arbitrarily set zero for convenience

$$F_{\min} = \sum_k (I_{exp,k}(E_{exp,k}) - I_{cal,k}(E_{exp,k}))^2 \quad (26)$$

$I_{exp,k}$ and $I_{cal,k}$ are the respective experimental and calculated current densities that correspond to a given potential $E_{exp,k}$, where k covers the whole experimental I–V pairs. Spline interpolation [38] is employed to retrieve $I_{cal,k}(E_{exp,k})$ *for each* $E_{exp,k}$. *Fixed kinetic and mass transport parameters used in the model are shown in Table 2.*

3 Results and discussion

3.1 Model prediction with uniform SPE distribution within the catalyst layer

3.1.1 Comparison with Qi and Kaufman's experimental work [6]

Figure 2 depicts a comparison of the model simulation with the experimental data of Qi and Kaufman [6]. A qualitative trend of the enhanced performance with larger platinum loadings for a fixed 30 wt% Nafion content is predicted. There is an early occurrence of limiting behavior for the lowest Pt loading of 0.074 mg cm^{-2} when the cell current density is increased. This is caused by the dominating oxygen diffusion limitation through the external SPE film covering the agglomerate slabs, which is significant at larger electrode over-potential. δ_n is 0.6480×10^{-4} cm at 30 wt% Nafion. The fitted parameters are as follows: $\kappa_m = 0.253 \times 10^{-1}$ S cm^{-1}, $D = 0.928 \times 10^{-5}$ cm^2 s^{-1}, and $j_{o,ref} = 0.181 \times 10^{-6}$ A cm^{-2}. In comparison with experiment the simulation shows an over-estimated current density at larger cell voltage but an under estimation at the intermediate potential when Pt loading is increased. Thus, an under-estimation of the polymer conductivity and an overestimation of the oxygen diffusivity within the electrolyte are anticipated due to the complex nature of the three-dimensional catalyst layer.

Table 2 Fixed parameters used in the model unless otherwise specified.

Nafion membrane thickness (Nafion®112), L_m	0.0051 cm
Density of platinum, ρ_{Pt}	21.5 g cm^{-3} [a]
Density of carbon, ρ_c	2 g cm^{-3} [a]
Density of solid polymer electrolyte, ρ_n	1.58 g cm^{-3} [b]
Proton diffusivity in polymer phase, D_{H+}	4.5×10^{-5} cm^2 s^{-1} [c]
Transfer coefficient of oxygen reduction, α	1 [a]
Void fraction of gas phase in gas diffuser, ε_d	0.6
Void fraction within the agglomerate, ε_a	0.3 [d]
Slab radius, δ	0.5×10^{-4} cm [e]
Slab inter-distance, δ_t	1.0×10^{-4} cm [f]
Catalytic area per gram of Pt in 40 wt% Pt/C, a_s	0.72×10^6 cm^2 g^{-1} [a]
Molecular weight of O_2, M_A	32 g mol^{-1} [g]
Molecular weight of N_2, M_B	28 g mol^{-1} [g]
Critical pressure of O_2, P_{CA}	49.7 atm [g]
Critical pressure of N_2, P_{CB}	33.5 atm [g]
Critical temperature of O_2, T_{CA}	154.4 K [g]
Critical temperature of N_2, T_{CB}	126.2 K [g]

[a] Ref. [16]

[b] Ref. [1]

[c] Ref. [17]

[d] Ref. [22]

[e] Chosen the same as the spherical agglomerate radius that used in Ref. [22]

[f] Chosen so that maximum gas void fraction is 0.5 when $\delta_n = \delta$ and no liquid water existed

[g] Ref. [35]

As a reference, the analytical limiting current density is derived in Appendix B (Eq. B7) as the function of bulk channel oxygen concentration, and gas diffuser and catalyst layer void structure characteristics. It is shown that the limiting current density can be expressed as the serial contributions of the oxygen diffusion through the gas diffuser, $1/_{d,lim}$, and that through the gas void in the catalyst layer as well as the external ionomer film on the agglomerates $1/[I_{c,lim} mL_c \tanh(mL_c)]$. I_{lim} estimated in Eq. B7 gives 0.5344, 1.016, 1.439, 1.929, and 2.335 A cm^{-2}, respectively for the given platinum loadings of 0.074, 0.147, 0.217, 0.306, and 0.387 mg cm^{-2}. The major oxygen transport resistance is the diffusion through the SPE film and that into the agglomerate slabs, while that from the gas phase in the pores of gas diffuser and catalyst layer are minor.

3.1.2 Transfer current density profiles within the catalyst layer

The oxygen reduction rate can be induced by the transfer current density profile, di/dx, as depicted in Fig. 3 at a cell

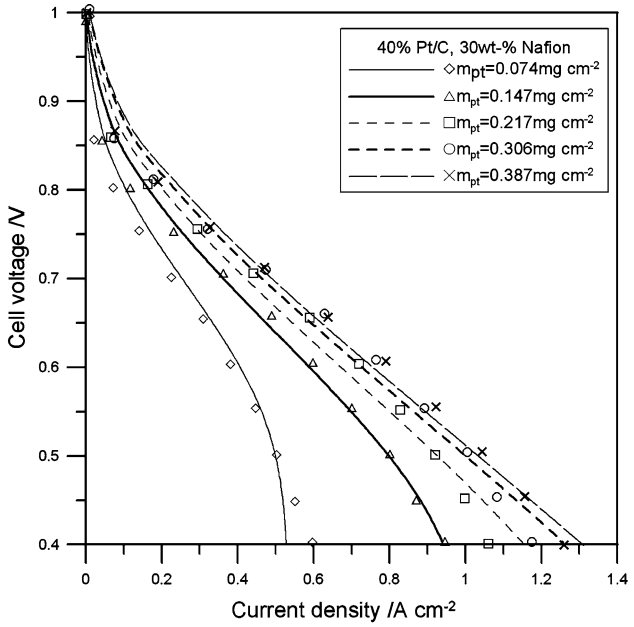

Fig. 2 Comparison of the experimental data (symbols) of Qi and Kaufman [6] with the model simulation (lines). SPE content in the catalyst layer is 30 wt%. Catalyst: 40 wt% Pt/C (E-TEK); gas diffuser: ELAT (E-TEK), L_d = 275 μm; membrane: Nafion® 112, L_m = 51 μm. Fitted parameters: $\kappa_m = 0.253 \times 10^{-1}$ S cm^{-1}, $D = 0.928 \times 10^{-5}$ cm^2 s^{-1}, and $j_{o,ref} = 0.181 \times 10^{-6}$ A cm^{-2}. Operating conditions: air feed in cathode (21% O_2, 79% N_2); temperatures of cell/anode/cathode = 35/45/45 °C, fully humidified anode and cathode feeds

potential of 0.6 V. The thickness of the catalyst layer is proportional to the Pt loading. Although a thinner catalyst layer suggests an easier migration of protons from the membrane side and a shorter gas diffusion length from the gas diffuser, the available active surface area for the electrochemical reaction is less. As indicated in the figure, the highest reaction rate is observed at a Pt loading of 0.074 mg cm^{-2}, while that at 0.387 mg cm^{-2} is the lowest. However, the larger total active surface area at higher platinum loadings results in a higher cell current density. Nonetheless, a diminished effect of increased platinum loading on cell performance is observed (also referred to Fig. 2).

3.1.3 *Electrolyte potential profiles within the catalyst layer*

Figure 4 shows the corresponding electrolyte potential profiles within the CL. The diminished effect of higher Pt loading on the enhancement of cell current density is due to the increased ohmic resistance across the thicker catalyst layer, and the migration of protons across the CL becomes more difficult. In general, a larger value of effective conductivity, κ_m^{eff}, a higher polymer electrolyte weight percentage and a thinner catalyst layer favor a lower ohmic drop ($\Delta\Phi$) across the CL.

3.1.4 *Gaseous oxygen concentration profiles within the catalyst layer*

The dimensionless gaseous oxygen concentration across the CL in Fig. 5 indicates that gas phase mass transfer resistance is very small. Since no water effect is included in the study, the concentration is overestimated due to the

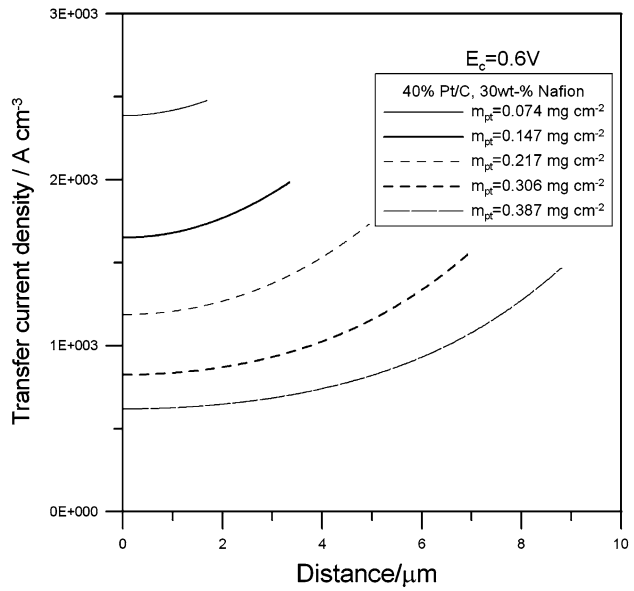

Fig. 3 Transfer current densities across the catalyst layer at E_c = 0.6 V. Operating conditions are the same as in Fig. 2

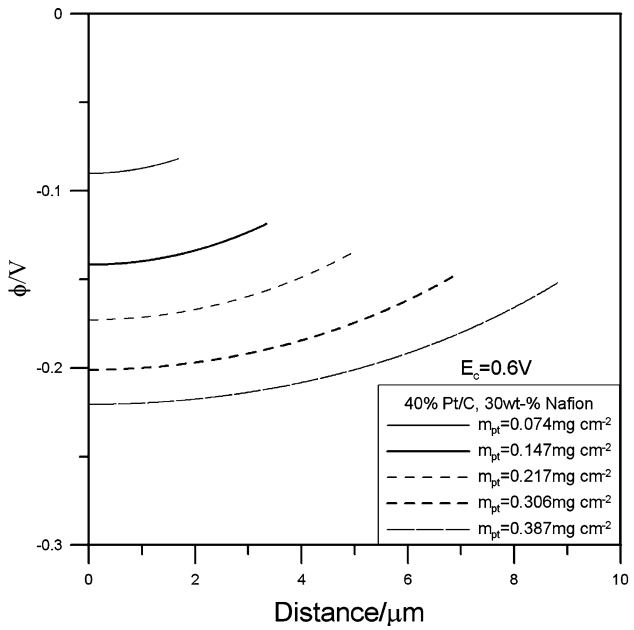

Fig. 4 Local electrolyte potential profiles in the catalyst layer at E_c = 0.6 V. Operating conditions are the same as in Fig. 2

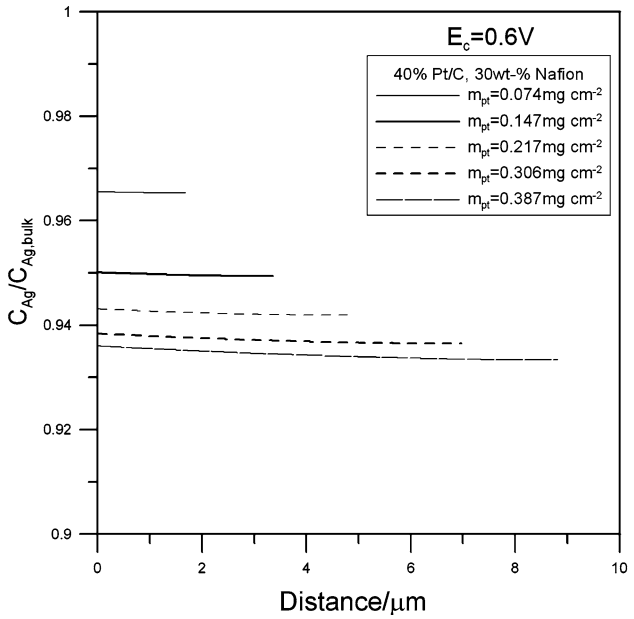

Fig. 5 Dimensionless oxygen gas concentration profiles in catalyst layer at E_c = 0.6 V. Operating conditions are the same as in Fig. 2

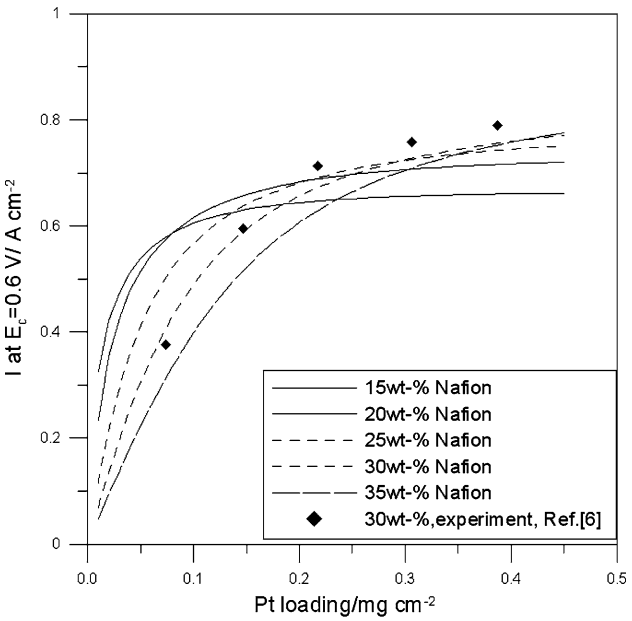

Fig. 6 Simulated cell current density at E_c = 0.6 V versus Pt loading at various Nafion contents in the catalyst layer. Symbol ◆ is for experimental data at 30 wt% Nafion content from Qi and Kaufman [6]. Operating conditions are the same as in Fig. 2

neglect of water vapor dilution and liquid water blocking in the voids. The effect of water could be significant at high current densities where flooding is likely to occur.

3.1.5 Effect of platinum loadings on the cell performance

It is interesting to view the platinum loading effect at various Nafion contents as shown in Fig. 6 at E_c specified at 0.6 V. It is observed that at low platinum loading, higher SPE content induces a lower cell current density. That is, the thicker external electrolyte film covering the agglomerate diminishes the oxygen mass transfer rate when higher ionomer content is used. A thin catalyst layer, corresponding to the low Pt loading, suggests efficient proton migration, and oxygen diffusion across the external polymer film becomes the controlling factor; as a consequence, too much Nafion content only increases the oxygen mass transfer barrier. On the other hand, at high catalyst loading of the thicker catalyst layer, axial proton migration becomes the dominant factor. Higher Nafion content improves proton migration when thicker CL is used. There are interesting intersections of cell current densities between two sequential electrolyte loadings, the locations of which shift in the direction of higher Pt loadings. Such observation suggests the existence of a competing effect of mass diffusion of oxygen through the catalyst slabs and proton migration across the catalyst layer. The intersection defines the regimes with regard to the relative importance of the two dominating factors. The physical significance of the experimental data of Qi and Kaufman [6] is included in Fig. 6, which can be qualitatively predicted by the model. It should be mentioned that the model results are based on a single loading of 40 wt% platinum Pt/C for the simplified thin-film/agglomerate structure. The experimental measured cell performance should be dependent on the actual three-dimensional catalyst layer structure, the fabrication method used, the platinum weight percentage in the catalyst and the relative amount of platinum and electrolyte. Passalacqua et al. [3] found that at a fixed platinum loading of 0.1 mg cm^{-2}, current declines when a large Nafion content is incorporated due to the limitation of oxygen transport within the electrolyte. A similar limitation was observed by Passos et al. [12], at a platinum loading of 0.4 mg cm^{-2}, which occurs at 35 wt% Nafion content at a prescribed cell voltage. In spite of the restrictions imposed, this model identifies major rate controlling factors within the CL. The predicted trends are consistent with much experimental work.

3.1.6 Effect of electrolyte composition on the cell performance

The relative importance of vertical oxygen diffusion through the catalyst agglomerate and the axial ohmic proton transport can be inferred from the polarization curve at various electrolyte contents depicted in Fig. 7. It is shown that at low over-voltages, for instance at E_c = 0.8 V, a higher SPE content enhances the reaction rate. For an intermediate potential at 0.6 V, an optimum content of

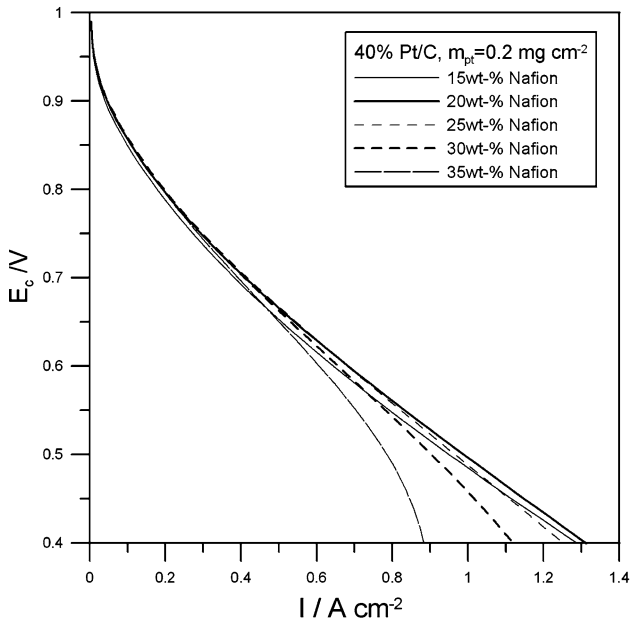

Fig. 7 Polarization curves of cell for 40 wt% Pt/C, platinum loading m_{pt} = 0.2 mg cm^{-2} at various Nafion contents. Operating conditions are the same as in Fig. 2

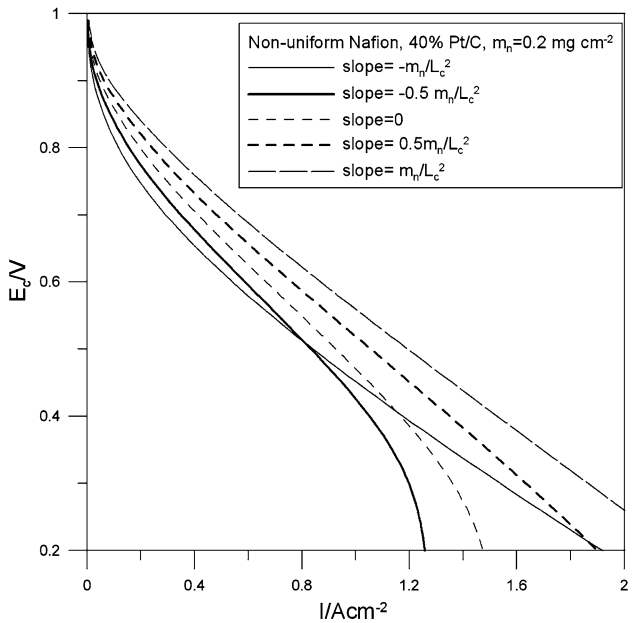

Fig. 8 Effect of non-uniform ionomer distribution on the cell performance. κ_m, D, and $j_{o,ref}$ and operating conditions are the same as that in Fig. 2. Ionomer loading m_n = 0.2 mg cm^{-2}, catalyst loading m_{pt} = 0.2 mg cm^{-2}, L_c calculated 4.55 μm. Linear distribution of ionomer is expressed as: $y/(m_n/L_c) = m(x/L_c - 0.5) + 1$, where y = local electrolyte weight density, x = position within the catalyst layer, and slopes m used are –1, –0.5, 0, 0.5, and 1, respectively

SPE is observed which is determined by the competing factors of oxygen diffusion and proton migration as discussed earlier. At the high over-potential of 0.4 V, the mass transfer inhibition of oxygen at high Nafion content is clear. As a reference, the limiting current densities are calculated according to Eq. B7. That is, 0.9188, 1.339, 2.219, and 5.215 A cm^{-2} for 35, 30, 25, and 20 wt% Nafion content, respectively. Since the model does not include possible water flooding effects, theoretical limiting current density should be larger than that actually measured. It is noted that the theoretical limiting current density for the Case II of insufficient electrolyte loading (15 wt% Nafion), Eq. B10 predicts a value of 11.81 A cm^{-2}. The only mass transfer resistance in such case is that from GDL. There is no contribution from the catalyst layer [25]; thus, $I_{lim} = I_{d,lim}$.

3.2 Model prediction with non-uniform SPE distribution within the catalyst layer

3.2.1 Model results on various electrolyte distributions at a specified Nafion loading

SPE distribution within the catalyst layer may be non-uniform due to different fabrication methods of the GDE. Fig. 8 is an illustration of cell performance for various linear density distributions of a SPE within the catalyst layer at a fixed Nafion loading of 0.2 mg cm^{-2}. The ionomer distribution is given as:

$$\frac{\text{ionomer weight density}}{m_n/L_c} = slope\left(\frac{x}{L_c} - 0.5\right) + 1 \qquad (27)$$

It is predicted that overall cell performance is favored by a more concentrated electrolyte near the membrane side. It is also noticed that a much lower limiting current density is observed when the SPE density is concentrated near the GDL/CL interface suggesting the more severe oxygen diffusion limitation there.

3.2.2 Transfer current density profiles within the catalyst layer

The local transfer current density profile sliced at E_c = 0.6 V is depicted in Fig. 9. Generally, a favorable reaction distribution is achieved with higher ionomer weight density near the membrane and higher current density is obtained as a result. On the other hand, average transfer current density is lower when the SPE is occupied near the gas diffusion layer. There is an interesting peak near the catalyst layer/membrane interface when SPE is concentrated near the GDL as most prominent at the *slope* = $-m_n/L_c^2$ in the electrolyte distribution of Eq. 27. This is caused by the competing effects of the faster oxygen mass transfer of a thin electrolyte barrier that is traded off by a larger

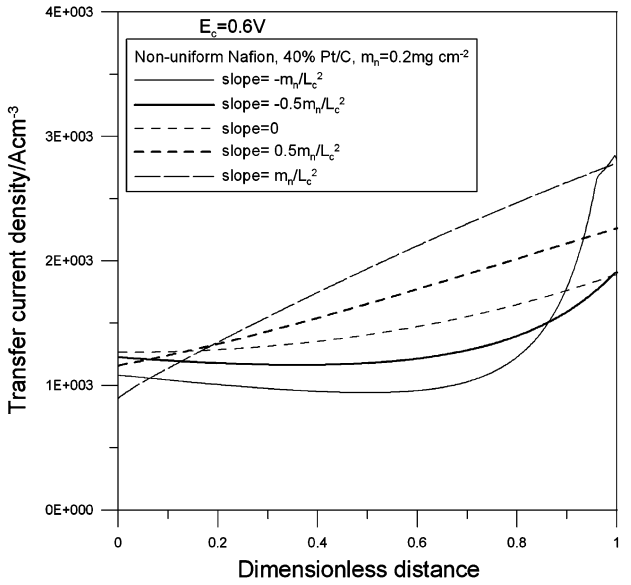

Fig. 9 Transfer current density profiles in the catalyst layer at E_c = 0.6 V. Key is as that in Fig. 8

ohmic resistance of low effective conductivity near the CL/M interface.

3.2.3 *Model fit to Yoon et al. data [7] with non-uniform electrolyte distribution within the catalyst layer*

Yoon et al. [7] fabricated GDEs with two different approaches. In the first method the gas diffusion layer was brushed with the catalyst slurry prepared by a solvent-added Pt/C paste followed by heat treatment. Diluted Nafion electrolyte solution was then sprayed onto the surface of the gas diffusion electrode. For the second method, a homogeneous mixture of Pt/C, solvent, and Nafion paste was prepared and brushed onto the gas diffusion together before the heat treatment. Apparently, a more concentrated electrolyte density occurs near the cathode CL/M interface of the finished MEA when using the first fabrication technique. The MEA prepared by the second method is expected to have a uniform electrolyte distribution in the catalyst layer. Since the precise SPE distribution in the catalyst layer is not experimentally available, we adopt a simple linear electrolyte distribution to simulate the cell I–V data for the GDE prepared by the first method as follows.

$$\text{SPE weight density} = a + b\frac{x}{L_c} \tag{28}$$

Polymer electrolyte loading, prescribed experimentally, is given by integrating Eq. 28 over the catalyst layer thickness.

$$a + \frac{b}{2} = \frac{m_n}{L_c} \tag{29}$$

In addition, the local SPE weight densities, expressed in Eq. 28, at $x = 0$ and $x = L_c$ are under the constraint of the local available void space. That is

$$0 < a < \rho_n n_s(\delta_t - \delta(1 - \varepsilon_a)) \tag{30}$$

$$0 < a + b < \rho_n n_s(\delta_t - \delta(1 - \varepsilon_a)) \tag{31}$$

Parameters a and b are determined by fitting the model to the measured polarization data using Eq. 26 and constraints (29), (30), and (31) with the aid of subprogram DNCONF which is capable of handling constrained minimization problems [38].

Figure 10 displays the experimental results in comparison with the theoretically predicted polarization behavior. As anticipated, a profound effect on the cell performance is

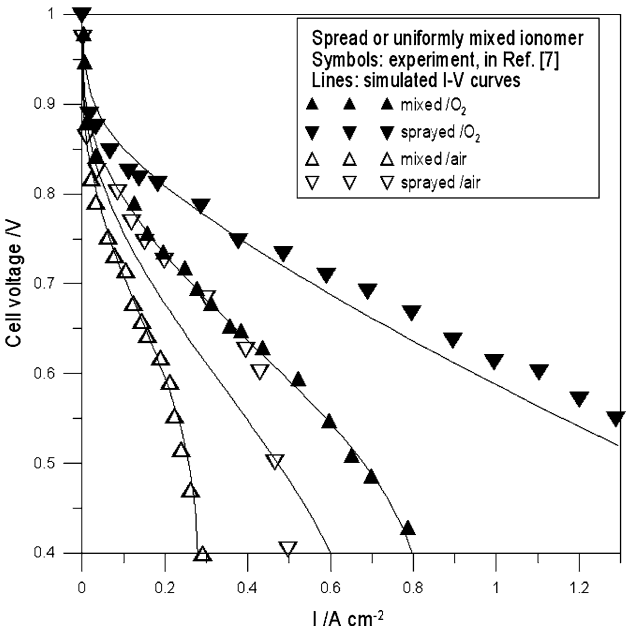

Fig. 10 Experimental data (symbols) of Yoon et al. [7] and the present simulation (lines). Gas diffuser: TGP-H-60 (Toray, L_d = 180 μm); catalyst: 40 wt% Pt/C HiSPEC4000 (Johnson Matthey); membrane: Nafion® 112, L_m = 51 μm; Nafion content: 35 wt% ionomer; Pt loading: 0.4 mg cm^{-2}. L_c calculated 9.1 μm. Operating conditions: temperatures of cell/anode/cathode = 60/70/70 °C, fully humidified in the anode and cathode feeds. Stoichiometry of H_2/O_2 or H_2/air =1.25/2.5. Symbols: ▲ uniformly mixed ionomer in the catalyst layer, oxygen feed; ▼ spray of ionomer onto the catalyst layer, oxygen feed; △ uniformly mixed ionomer in the catalyst layer, air feed; ▽ spray of ionomer onto the catalyst layer, air feed. Fitted parameters for the catalyst layer with uniform electrolyte distribution: $\kappa_m = 0.366 \times 10^{-1}$ S cm^{-1}, $D = 0.981 \times 10^{-6}$ cm^2 s^{-1}, $j_{o,ref} = 0.350 \times 10^{-8}$ A cm^{-2} with pure oxygen feed, and $\kappa_m = 0.227 \times 10^{-1}$ S cm^{-1}, $D = 0.159 \times 10^{-5}$ cm^2 s^{-1}, $j_{o,ref} = 0.914 \times 10^{-8}$ *A cm^{-2} with air feed.* κ_m, *D, and* $j_{o,ref}$ *retrieved from the uniform ionomer distributed catalyst layer are adopted for the non-uniform electrolyte distributed catalyst layer. Fitted linear electrolyte weight density profile for pure oxygen feed is 0.156 + 0.871(x/L$_c$), and that for air feed is 0.361+0.462(x/L$_c$)*

found as a consequence of the electrolyte distribution due to different GDE preparations. The cell current density is higher if theGDE is prepared by the first method as compared to that using the second method of well-mixed electrolyte in the catalyst layer. For the Nafion-spray prepared GDE, it is believed that the SPE is more concentrated near the outer surface of the cathode GDE. Hence, the SPE density is higher near the cathode catalyst layer/membrane interface as a complete MEA is assembled.

4 Conclusion

A thin-film/agglomerate model of the cathode catalyst layer of a PEMFC is proposed. Parameters of oxygen diffusivity within the polymer electrolyte D, proton conductivity κ_m, and exchange current density of oxygen reduction $j_{o,ref}$can be estimated by fitting available experimental data with the model. It is shown that the cell performance can be correlated well with the electrolyte content and its distribution within the catalyst layer. Two important factors determine the resultant cell performance, that is, the radial diffusion of oxygen through the agglomerate and the axial proton migration across the catalyst layer. It is found that the non-uniform electrolyte distribution concentrated near the catalyst layer/membrane interface enhances the overall cell performance.

Acknowledgements A grant from National Science Council of the Republic of China (NSC-94-2214-E-155-003) is much appreciated. The author is indebted to Li-Li Cheng for the assistance in numerous aspects of the study. Figure 1 was prepared by J.-H. Chien.

Appendix A: Dimensional analysis of the catalyst layer

The number of slabs per unit cross sectional area n_s, catalyst layer thickness L_c, and ionomer occupied thickness δ_n can be deduced, once the platinum loading m_{pt}, ionomer loading m_n, void fraction within the agglomerate ε_a, agglomerate size δ, and geometrical parameter δ_t, are specified.

The number of slabs per unit area n_s is related to δ_t

$$n_s = \frac{1}{\delta_t} \tag{A1}$$

For $\delta_n > \delta$ (Case I) volume conservation on the Pt/C/electrolyte phase gives

$$L_c n_s \delta_n = \frac{m_n}{\rho_n} + \frac{m_{pt}}{\rho_{pt}} + \frac{m_{pt}}{w}\frac{1-w}{\rho_c} \tag{A2}$$

and volume conservation on the Pt/C phase is

$$L_c n_s \delta (1-\varepsilon_a) = \left(\frac{m_{Pt}}{\rho_{pt}} + \frac{m_{pt}}{w}\frac{1-w}{\rho_c}\right) \tag{A3}$$

Combination of (A2) and (A3) gives

$$\frac{\delta_n}{\delta} = \frac{\left(\frac{m_n}{\rho_n} + \frac{m_{pt}}{\rho_{pt}} + \frac{m_{pt}}{w}\frac{1-w}{\rho_c}\right)(1-\varepsilon_a)}{\frac{m_{pt}}{\rho_{pt}} + \frac{m_{pt}}{w}\frac{1-w}{\rho_c}} \tag{A4}$$

For $\delta_n < \delta$ (Case II) volume conservation on the Pt/C/electrolyte phase is

$$L_c n_s \delta_n = \frac{m_n}{\rho_n \varepsilon_a} \tag{A5}$$

Combination of (A3) and (A5) gives

$$\frac{\delta_n}{\delta} = \frac{m_n(1-\varepsilon_a)/(\rho_n \varepsilon_a)}{\frac{m_{pt}}{\rho_{pt}} + \frac{m_{pt}}{w}\frac{1-w}{\rho_c}} \tag{A6}$$

Note the expression of L_c in (A3) is applicable to both cases.

The active area per unit volume of Pt/C/ionomer mixed region, a_v, for both cases is simply

$$a_v = \frac{m_{pt} a_s}{\delta L_c n_s} \tag{A7}$$

Appendix B: Limiting current density expression

The limiting current density of fuel cell for Case I can be derived by letting $C_{A\delta} = 0$ everywhere across the catalyst layer. The local transfer current density becomes

$$\frac{di}{dx} = -a_e n F \frac{D C_{Ag}}{\delta_f K_A} \tag{B1}$$

where a_e is the slab external area density (the gas/electrolyte interfacial area per unit volume of the catalyst layer). As suggested in (A1),$a_e = n_s L_c / L_c = 1/\delta_t$.

(B1) is to be combined with Eq. 17 to give

$$\frac{d^2 C_{Ag}}{dx^2} - \frac{D}{D_g^{eff} \delta_t \delta_f K_A} C_{Ag} = 0 \tag{B2}$$

Let $\frac{dC_{Ag}}{dx}(x = L_c) = 0$, the solution to (B2) is

$$C_{Ag} = C_{Ag}(x=0)[\cosh(mx) - \tanh(mL_c)\sinh(mL_c)] \tag{B3}$$

where

$$m = \sqrt{\frac{D}{D_g^{eff}\delta_t\delta_f K_A}} \tag{B4}$$

Integration of (B1) across the catalyst layer thickness with the aid of (B3), gives the limiting current density

$$I_{lim} = -\frac{nFDL_c}{\delta_t\delta_f K_A} C_{Ag}(x=0)\frac{\tanh(mL_c)}{mL_c} \tag{B5}$$

C_{Ag} at GDL/CL interface ($x = 0$) can be correlated to the bulk concentration in the flow channel

$$C_{Ag}(x=0) = C_{Ag,bulk}(x=-L_d) + \frac{I_{lim}L_d}{nFD_{gd}^{eff}} \tag{B6}$$

Finally, the limiting current density is rearranged as

$$\frac{1}{I_{lim}} = \frac{1}{I_{c,lim}mL_c\tanh(mL_c)} + \frac{1}{I_{d,lim}} \tag{B7}$$

where

$$I_{c,lim} = -\frac{nFD_g^{eff}C_{Ag}(x=-L_d)}{L_c} \tag{B8}$$

$$I_{d,lim} = -\frac{nFD_{gd}^{eff}C_{Ag}(x=-L_d)}{L_d} \tag{B9}$$

$I_{c,lim}mL_c\tanh(mL_c)$ can be viewed as the mass transfer resistance in the CL region, while $I_{d,lim}$ is that from the GDL.

For Case II, when the SPE loading is insufficient to fill the voids of the agglomerate particles, there is no theoretical mass transport limitation from the CL. As a result, the limiting current density is merely determined from mass transfer through the GDL [25]:

$$I_{lim} = I_{d,lim} \tag{B10}$$

References

1. Lee SJ, Mukerjee S, McBreen J, Rho YW, Kho YT, Lee TH (1998) Electrochim Acta 43:3693
2. Passalacqua E, Lufrano F, Squadrito G, Patti A, Giorgi L (1998) Electrochim Acta 43:3665
3. Passalacqua E, Lufrano F, Squadrito G, Patti A, Giorgi L (2001) Electrochim Acta 46:799
4. Antolini E, Giorgi L, Pozio A, Passalacqua E (1999) J Power Sources 77:136
5. Song JM, Cha SY, Lee WM (2001) J Power Sources 94:78
6. Qi Z, Kaufman A (2003) J Power Sources 113:37
7. Yoon YG, Yang TH, Park GG, Lee WY, Kim CS (2003) J Power Sources 118:189
8. Sasikumar G, Ihm JW, Ryu H (2004) J Power Sources 132:11
9. Sasikumar G, Ihm JW, Ryu H (2004) Electrochim Acta 50:601
10. Xie Z, Navessin T, Shi K, Chow R, Wang Q, Song D, Andreaus B, Eikerling M, Liu Z, Holdcroft S (2005) J Electrochem Soc 152(6): A1171
11. Song Y, Xu H, Wei Y, Kunz HR, Bonville LJ, Fenton JM (2006) J Power Sources 154:138
12. Passos RR, Paganin VA, Ticianelli EA (2006) Electrochim Acta 51:5239
13. Park GG, Sohn YJ, Yang TH, Yoon YG, Lee WY, Kim CS (2004) J Power Sources 131:182
14. Wang X, Zhang H, Zhang J, Xu H, Zhu X, Chen J, Yi B (2006) J Power Sources 162:474
15. Cheddie D, Munroe N (2005) J Power Sources 147:72
16. Marr C, Li X (1999) J Power Sources 77:17
17. Bernardi DM, Verbrugge MW (1991) AIChE J 37:1151
18. Bernardi DM, Verbrugge MW (1992) J Electrochem Soc 139:2477
19. Springer TE, Wilson MS, Gottesfeld S (1993) J Electrochem Soc 140:3513
20. Wang Q, Eikerling M, Song D, Liu Z, Navessin T, Xie Z, Holdcroft S (2004) J Electrochem Soc 151(7):A950
21. Hsuen HK (2003) J Power Sources 123:26
22. Broka K, Ekdunge P (1997) J Appl Electrochem 27:281
23. Siegel NP, Ellis MW, Nelson DJ, von Spakovsky MR (2003) J Power Sources 115:81
24. Wei ZD, Ran HB, Liu XA, Liu Y, Sun CX, Chan SH, Shen PK (2006) Electrochim Acta 51:3091
25. Springer TE, Raistrick ID (1989) J Electrochem Soc 136:1594
26. Raistrick ID (1990) Electrochim Acta 35:1579
27. Perry ML, Newman J, Cairns EJ (1998) J Electrochem Soc 145:5
28. Jaouen F, Lindbergh G, Sundholm G (2002) J Electrochem Soc 149(4):A437
29. Wang Q, Song D, Navessin T, Holdcroft S, Liu Z (2004) Electrochim Acta 50:725
30. Song D, Wang Q, Liu Z, Navessin T, Holdcroft S (2004) Electrochim Acta 50:731
31. Yin KM (2005) J Electrochem Soc 152(3):A583
32. Pisani L, Murgia G, Valentini M, D'Aguanno B (2002) J Electrochem Soc 149(7):A898
33. Pisani L, Valentini M, Murgia G (2003) J Electrochem Soc 150(12):A1549
34. Lin G, He W, Nguyen TV (2004) J Electrochem Soc 151(12):A1999
35. Bird RB, Stewart WE, Lightfoot EN (1960) Transport phenomena. Wiley, New York
36. Bard AJ, Faulkner LR (1980) Electrochemical methods: fundamentals and applications. Wiley, New York
37. Newman JS (1991) Electrochemical system. Prentice-Hall, Englewood Cliffs NJ
38. User's Manual (1996) IMSL Math/Library, Version 3, Visual numerics, Houston